1. Piya SIRIKAN[1], 2. Chakrapong CHARUMIT[1]

Pathumwan Institute of Technology, Thailand
ORCID. 1. 0000-0001-8688-7607, 2. 0000-0002-0762-2588

Analytical Performance Investigation of Unsymmetrical Two-Phase Induction Motor Drives using Indirect RFOC Strategy Under Unbalanced Voltage Supply Conditions

Abstract. *This paper presents an investigation and a performance evaluation of an unsymmetrical two-phase induction motor (U-TPIM) controlled by an indirect rotor flux orientation (IRFO) strategy under the difference of stator winding voltages using the unbalanced space vector PWM technique. The main and auxiliary windings are fed by the appropriate voltages as the correct proportion of an effective turns ratio between the auxiliary and main windings so as to eliminate the backward rotating field, reduce the torque pulsation and increase the electromagnetic torque. In addition, this effective turns ratio is employed for the similar magnitude compensation of stator winding currents in rotor flux oriented control. Thus, the double line frequency components established by an unsymmetrical component of the stator current transformation in the rotating reference frame are eliminated. To confirm the validity, the comprehensive simulation results using Matlab/Simulink are illustrated, and the experimental results implemented by dSPACE illustrate the speed response, electromagnetic torque, currents and voltages in the stationary and rotating reference frame. All of the established experimental results indicate that the proposed U-TPIM performances are improved.*

Streszczenie. *W artykule przedstawiono badanie i ocenę działania niesymetrycznego dwufazowego silnika indukcyjnego (U-TPIM) sterowanego za pomocą strategii pośredniej orientacji strumienia wirnika (IRFO) w warunkach różnicy napięć uzwojenia stojana przy użyciu techniki niezrównoważonego wektora przestrzennego PWM. Uzwojenia główne i pomocnicze są zasilane odpowiednimi napięciami, jako właściwa proporcja efektywnego stosunku zwojów między uzwojeniem pomocniczym i głównym, tak aby wyeliminować wsteczne pole wirujące, zmniejszyć pulsacje momentu obrotowego i zwiększyć moment elektromagnetyczny. Ponadto ten efektywny współczynnik zwojów jest wykorzystywany do kompensacji podobnej wielkości prądów uzwojenia stojana w sterowaniu zorientowanym na strumień wirnika. W ten sposób eliminowane są składowe podwójnej częstotliwości linii ustalone przez niesymetryczną składową transformacji prądu stojana w wirującym układzie odniesienia. Aby potwierdzić wiarygodność, zilustrowano kompleksowe wyniki symulacji z wykorzystaniem Matlab/Simulink, a wyniki eksperymentalne zaimplementowane przez dSPACE ilustrują odpowiedź prędkości, moment elektromagnetyczny, prądy i napięcia w stacjonarnej i obrotowej ramce odniesienia. Wszystkie ustalone wyniki eksperymentalne wskazują, że proponowane osiągi U-TPIM uległy poprawie. (**Badanie wydajności niesymetrycznych dwufazowych silników indukcyjnych przy użyciu pośredniej strategii RFOC w warunkach niesymetrycznego zasilania napięciem**)*

Keywords: Unbalanced two-phase induction motor, Indirect rotor field orientation, Single-phase induction motor, variable speed drive.
Słowa kluczowe: dwufazowy silnik indulkcyjny, napęd oróżnej prędkości

Introduction

The majority of permanently spit capacitor (PSC) motor applications are at a fixed speed operation, unlike the three-phase induction motors that can be used for variable speed drive. In order to save energy and adjust speed of the PSC motor like a three-phase induction motors, the start and run capacitors need to be cut out, because its capacitance will be changed when the line frequency is adjusted. Several papers have been proposed the modifications of PSC motors as unsymmetrical two-phase motor (U-TPIM) by removing a capacitor out from the auxiliary winding and separating main and auxiliary windings to improve the starting torque and variable speed drive. Since main winding differs from the auxiliary winding in terms of wire size and the number of turns thus resulting in unsymmetrical impedances and unbalanced stator magnetomotive forces. This results in increased high torque pulsation and low starting torque. To eliminate the oscillation term of the electromagnetic torque, main and auxiliary winding voltages are supplied by unbalanced two-phase voltage established by the unbalanced voltage source inverters [1]-[4].

The scalar control techniques of U-TPIM drives, the unbalanced two-phase voltages using sinusoidal pulse width modulation (SPWM) techniques were proposed in [1], [4]-[6], and the space vector PWM strategies have been reported in [3], [8]. Another approach of variable speed drive technique for U-TPIM is a vector control by the current control techniques providing a higher performance control [9]-[12].

Nowadays, vector control strategies for the U-TPIM have serious problems, as a result of which the impedances of both windings are unequal thus resulting in asymmetry of magnitude stator currents [12]. This problem leads to unbalanced magnitude currents of a stationary reference frame transformation and AC double line frequency in rotating reference frame transformation. Because of this, AC components (double line frequency currents) will be generated and appearing superimposed on the DC current components in rotating reference frame led to an increase in the AC term of electromagnetic torque.

There are a few published papers that did reveal the vector control methods for U-TPIM by controlling the voltage and current that is fed to both unbalanced windings using the effective turns ratio [9]-[11]. However, there are not any publication that analyzed the difference of unbalanced voltage supply adjustment using an effective turns ratio to find the lowest torque pulsation for the indirect

rotor flux oriented control. Hence, this paper focuses on U-TPIM adapted from an existing capacitor start and run motor by cutting out of the two-value capacitor. In this case, the auxiliary winding stayed in operation all the time, unlike the spit-phase and capacitor-start motor that the auxiliary winding will be cut off at about 75 percent of the synchronous speed. Moreover, this paper aims to investigate the indirect rotor field oriented control for U-TPIM focused on the balanced transforming of the stationary and rotating reference frame to reduce the torque pulsations. The Matlab/Simulink is used for a demonstration of simulation- based results, and dSPACE (MicroLabBox) is used for the implementation. For the experimental results, the U-TPIM performances of the proposed indirect rotor field-oriented control are illustrated in terms of a torque-speed control, four-quadrants operation, torque pulsation reduction, stator voltages and current waveforms in stationary and rotating reference frames.

Equivalent circuits of U-TPIM

For the symmetrical two-phase induction motor (TPIM), the main and auxiliary windings are identical in terms of wire size and number of turns. So, the number of turns of both windings is indicated by Nq (equivalent number of main winding turns) and Nd (equivalent number of auxiliary winding turns) as shown in Fig. 1(a). Both windings are placed in the stator as orthogonal to each other. Assume that the two-phase motor is connected to a two-phase supply which has a phase shift of 90 electrical degrees. As a result, the stator currents flowing through both windings are also orthogonal to each other. Analysis by employing the rotating magnetic field theory for the symmetrical TPIM is shown in Fig. 1(a). The forward rotating field components of main and auxiliary windings are defined as a $\phi_{m,f}$ and $\phi_{a,f}$, respectively. There are only the forward rotating field components in each of the windings because the summation of backward rotating fields is equal to zero [13]-[14].

On the other hand, the schematic diagram of the unsymmetrical two-phase motor as shown in Fig. 1(b) illustrates the difference of impedances of both windings. For this reason, the summation of backward rotating fields on the main winding $\phi_{m,b}$ and the auxiliary winding $\phi_{a,b}$ are not equal to zero. In addition, backward rotating fields produce the backward rotating torque and pulsating torque leading to a decrease in starting torque and an increase in pulsating torque.
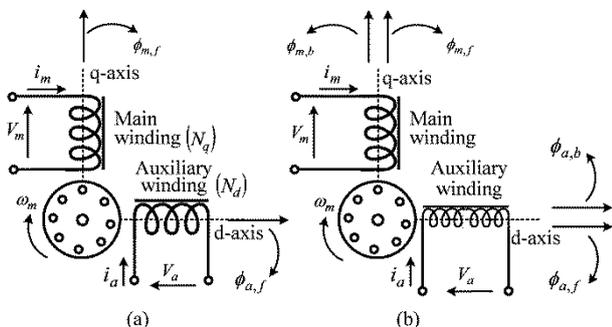

Fig. 1. Schematic diagrams of two-phase machine and its revolving magnetic field: (a) Symmetrical two-phase induction motor,
(b) Asymmetrical two-phase induction motor.

In the schematic diagrams of the U-TPIM as shown in Fig. 1(b), the number of turns for the auxiliary winding is higher than the number of turns for the main winding. The mathematical calculation of the U-TPIM equivalent circuit

has a difference from the symmetrical TPIM [14], [15]. In a stationary reference frame, a superscript "s" represents variables in the d^s-q^s axes. The main winding variables will be denoted as the q^s axis, and the auxiliary winding variables referred to the main winding represent the variables in d^s axis. As shown in Fig. 2, the approximate equivalent circuit of rotor winding consisting of N_r, R_r and x_{lr} are defined to be the effective number of turns, rotor winding resistance and rotor winding leakage reactance, respectively. All parameters of the rotor winding are referred to the main winding by ideal transformer using effective turns ratio of a main to rotor windings (N_q/N_r). According to Fig. 2, the rotor winding resistance and rotor winding leakage reactance are referred to main winding to be $R'_{r,m}$ and $x'_{lr,m}$, respectively. Note that the impedance of the rotor winding referred to the main winding is aligned with the quadrature axis.
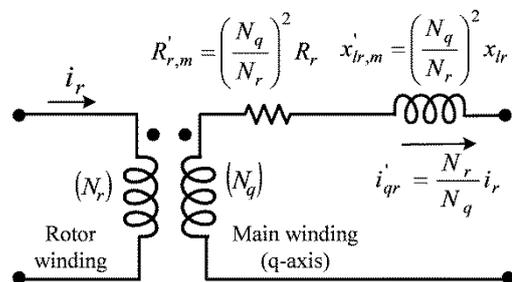

Fig. 2. Equivalent circuit of rotor winding referred to main winding in q-axis.

Likewise, the rotor winding parameters referred to the auxiliary winding are shown in Fig. 3(a), and rotor winding variables are referred to auxiliary winding by the ideal transformer using effective turns ratio of auxiliary to rotor windings (N_d/N_r). Thus, the rotor winding resistance and rotor winding leakage reactance referred to auxiliary winding are indicated by $R'_{r,a}$ and $x'_{lr,a}$, respectively. As shown in Fig. 3(b), the impedances of rotor side referred to auxiliary winding, afterward, auxiliary winding parameters referred to main winding are aligned with the direct axis by the effective turns ratio of main to auxiliary windings (N_q/N_d). Then, the auxiliary winding (rotor parameters) referred to main winding can be expressed as

(1) $$R''_{r,a} = \left(\frac{N_q}{N_d}\right)^2 R'_{r,a} = \left(\frac{N_q}{N_r}\right)^2 R_r$$

(2) $$x''_{lr,a} = \left(\frac{N_q}{N_d}\right)^2 x'_{lr,a} = \left(\frac{N_q}{N_r}\right)^2 x_{lr}$$

The rotor current (i_r) referred to auxiliary winding, afterward, referred to the main winding is

(3) $$i''_{dr} = \left(\frac{N_d}{N_q}\right)i'_r = \left(\frac{N_r}{N_q}\right)i_r$$

Referring to Fig. 2 and Fig. 3(b), $R'_{r,m}$ and $x'_{lr,m}$ are parameters of main winding in q-axis; $R''_{r,a}$ and $x''_{lr,a}$ are parameters of main winding in d-axis. Note that these parameters of rotor side are identical values as shown in

Figs. 4(a) and 4(b). Moreover, the rotor currents, i'_{dr} of main winding in q-axis and i''_{dr} of main winding in d-axis are also equal. From Eqs. (1)-(3), it can be noted that rotor winding parameters side in direct and quadrature axes are same in the quantities. Consequently, rotor winding resistance ($R'_{r,m}$ and $R''_{r,a} = R'_r$), rotor winding leakage reactance ($x'_{lr,m}$ and $x''_{lr,a} = x'_{lr}$) and rotor current ($i''_{dr} = i'_{qr}$ and $i'_{dr} = i'_{qr}$) are shown in Fig. 4. For the stator side of d-axis as shown in Fig. 4(b), auxiliary winding resistance R'_{ds}, auxiliary winding leakage reactance x'_{lds} and d-axis stator voltage $v^{s'}_{ds}$ are aligned with the direct-axis referred from the auxiliary winding to main winding by effective turns ratio N_q/N_d obtained as

(4) $\qquad R'_{ds} = \left(\dfrac{N_q}{N_d} \right)^2 R_{ds} \ ; \ x'_{lds} = \left(\dfrac{N_q}{N_d} \right)^2 x_{lds}$

(5) $\qquad v^{s'}_{ds} = \dfrac{N_q}{N_d} v^s_{ds} = \dfrac{1}{K_{eff}} v^s_{ds}$

(a)

$$R'_{r,a} = \left(\frac{N_d}{N_r} \right)^2 R_r \quad x'_{lr,a} = \left(\frac{N_d}{N_r} \right)^2 x_{lr}$$

$$i'_r = \frac{N_r}{N_d} i_r$$

(b)

$$R''_{r,a} = \left(\frac{N_q}{N_r} \right)^2 R_r \quad x''_{lr,a} = \left(\frac{N_q}{N_r} \right)^2 x_{lr}$$
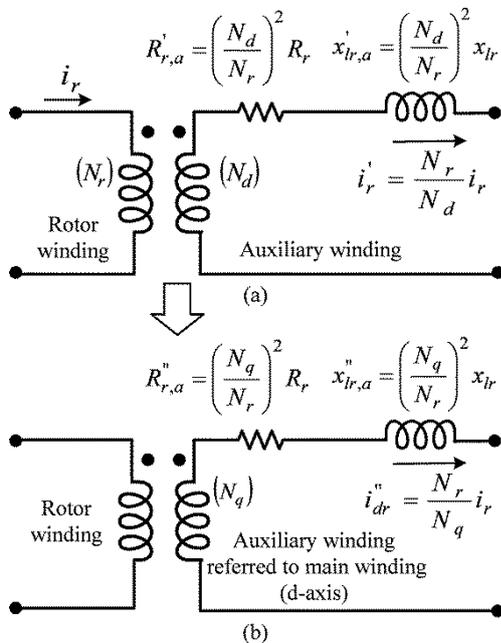
$$i''_{dr} = \frac{N_r}{N_q} i_r$$

Fig. 3. Equivalent circuits of auxiliary winding referred to main winding: (a) Rotor winding referred to auxiliary winding, (b) Auxiliary winding referred to main winding in d-axis.

According to the equivalent circuit in a stationary reference frame as shown in Fig. 4, the electromagnetic torque in the stationary reference frame with respect to stator and rotor currents can be obtained by

(6) $\qquad T_{em} = \dfrac{P}{2} L_m \left(i^s_{qs} i'^s_{dr} - i'^s_{ds} i'^s_{qr} \right)$

The corresponding torque in terms of stator flux vectors and stator currents in a stationary reference frame is expressed as

(7) $\qquad T_{em} = \dfrac{P}{2} \left(\lambda'^s_{ds} i'^s_{qs} - \lambda^s_{qs} i'^s_{ds} \right)$
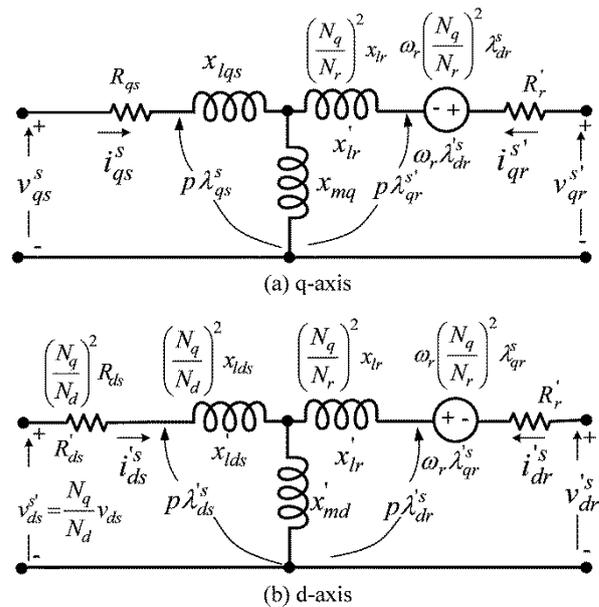

(a) q-axis

(b) d-axis

Fig. 4. Equivalent circuits of U-TPIM in stationary reference frame: (a) Main winding variables in q-axis, (b) Auxiliary winding variables referred to main winding in d-axis.

Proposed vector control technique for U-TPIM drive

In order to achieve the indirect RFOC for U-TPIM as well as the three-phase induction motor, the equivalent circuit parameters of U-TPIM need to be compensated as symmetrical equivalent circuit component by using the factor K_{eff}. Fig. 5 shows the proposed indirect RFOC system for U-TPIM. This system consists of the two-phase voltage supply fed U-TPIM by using a three-leg voltage source inverter based on an unbalanced voltage space vector pulse width modulation technique and the mathematical calculation block of indirect rotor field-oriented controller implemented by dSPACE. In addition, the proposed indirect RFOC system is also divided into two parts for instance balanced and unbalanced zones. Both zones are divided along a dashed line by multiplying the factor K_{eff} into direct axis of voltage and current. Many works presented the effective turns ratio with regard to the difference of number of turns and mutual inductances of both winding by neglecting the winding pitch and distribution factor [12]. However, it is difficult to calculate the correct effective turns ratio.

For the proposed factor K_{eff} calculation in this paper, the motor has to be controlled by the rotor speed at synchronous speed by coupling together with a servo motor acting as a prime mover to control the slip speed to become zero. For measuring of auxiliary winding induced voltage, only main winding is energized at rated voltage supply (E_m), and induced voltage (E'_a) of the auxiliary winding side is measured. In the same way, for the main winding induced voltage measurement (E'_m), the auxiliary winding is energized at a rated voltage supply (E_a). The effective turns ratio (N_d / N_q) can be expressed as

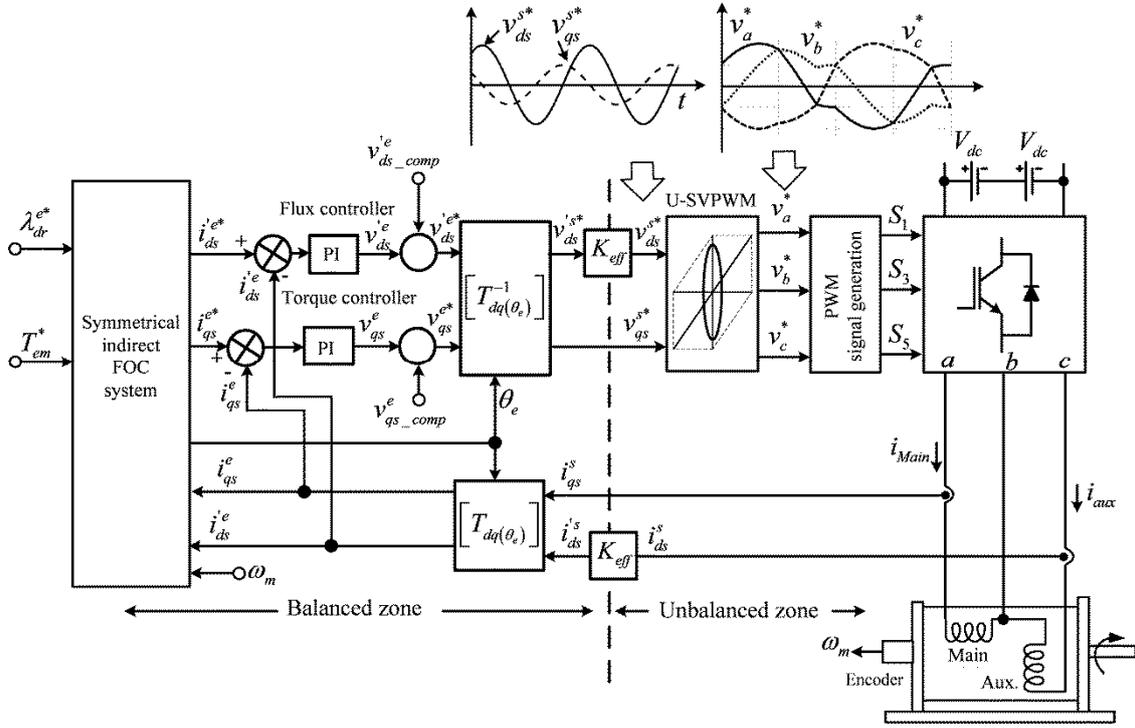(8) $\qquad K_{eff} = \sqrt{\dfrac{E'_a \, E_a}{E_m E'_m}}$

Fig. 5. Proposed indirect rotor field-oriented control system based on unbalanced voltage supply condition.

Unbalanced voltage SVPWM technique

According to an unbalanced zone in Fig. 5, the block diagram consists of a three-leg VSI modulated by unbalanced output voltage space vector (U-SVPWM) technique which was reported in Ref. [3]. Unbalanced two-phase voltages lead to eradicate the torque pulsation and improve speed regulation with excellent transient performance. The voltage across auxiliary winding needs higher than the main winding voltage as the factor K_{eff}.

The proposed three-leg VSI in this paper deals with the carrier based space vector PWM technique which is suitable for implementation by dSPACE. As shown in Fig. 5, command voltages v'^{s*}_{ds} and v^{s*}_{qs} in a stationary reference frame have the same magnitude, whereas v^{s*}_{ds} is determined as the auxiliary winding voltage having more magnitude than v'^{s*}_{ds} by multiplying the factor K_{eff}. Consequently, the magnitude of auxiliary winding voltage (v^{s*}_{ds}) and main winding voltage (v^{s*}_{qs}) are unequal. For unbalanced two-phase output voltages using three-leg VSI fed to U-TPIM, the mathematical functions of carrier based for unbalanced SVPWM and the relationship between two-phase and three-phase reference voltages can be written in a matrix form as

$$(9) \quad \begin{bmatrix} v^*_a \\ v^*_b \\ v^*_c \end{bmatrix} = \begin{bmatrix} 1 & 0 & -1 \\ 0 & 0 & -1 \\ 0 & 1 & -1 \end{bmatrix} \begin{bmatrix} (K_{eff})v^{s*}_{ds} \\ v^{s*}_{qs} \\ v_z \end{bmatrix}$$

where

Zero voltage; $v_z = \dfrac{(V_{max}) + (V_{min})}{2}$

V_{max} = Maximum of $\left((K_{eff})v^{s*}_{ds}, v^s_{qs}, 0\right)$

V_{min} = Minimum of $\left((K_{eff})v^{s*}_{ds}, v^s_{qs}, 0\right)$

K_{eff} = Magnitude of $v^{s*}_{ds} / v^{s*}_{qs}$

The DC bus voltage at maximum modulation index can be calculated as

$$(10) \quad \text{DC Bus voltage} = 2V_{dc} = \sqrt{\left(V^{s*}_{ds}\right)^2 + \left(V^{s*}_{qs}\right)^2}$$
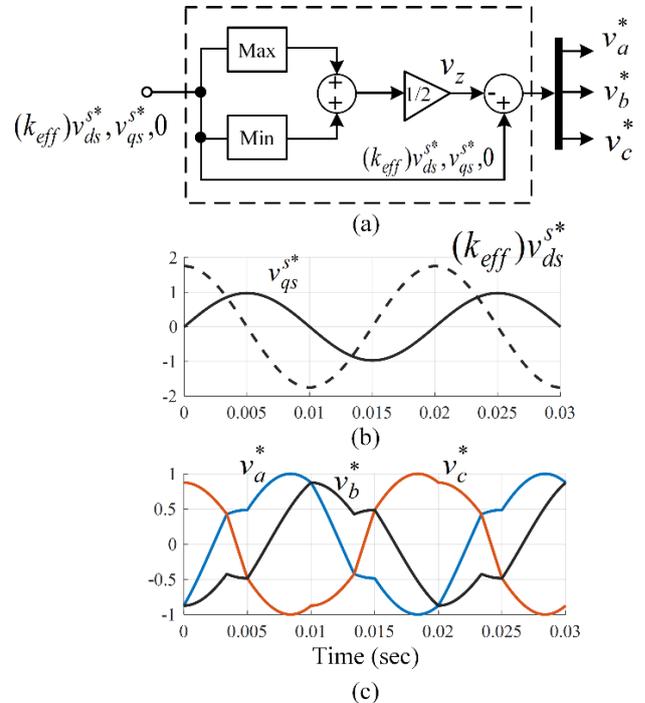

Fig. 6. Unbalanced 2-phase to 3-phase transformation system in a stationary reference frame. (a) Block diagram of 2-phase to 3-phase (b) Normalized two-phase voltage with respect to the midpoint of DC bus voltage (c) Normalized three phase-leg reference voltage space vector.

According to Eq. (9), three-phase reference voltages of carrier-based SVPWM signals can be implemented by the Simulink blockset as shown in Fig. 6(a). For example, The normalized input voltages of main and auxiliary windings in stationary reference frame are shown in Fig. 6(b). From matrix transformation Eq. (9), substituting the normalized two-phase voltages into Eq. (9), the normalized three-phase reference waveforms are plotted in Fig. 6(c). In addition, these phase-leg reference voltages will be compared with the carrier signal to generate the SVPWM gate driver signals.

Indirect rotor field-oriented control system

Like a separately excited DC motor control, rotor field oriented control of U-TPIM needs to control decoupling the torque and rotor flux vector independently [14]- [16]. Thus, the equivalent circuits in the stationary reference frame according to Fig. 4 modified as rotating reference frame are shown in Fig. 7. The torque equation in the rotating reference frame can be rewritten as

$$(11) \qquad T_{em} = \frac{P}{2}\left(\lambda_{dr}^{'e} i_{qs}^{e} - \lambda_{qr}^{'e} i_{ds}^{'e} \right)$$

Under the field oriented control condition, the rotor flux vector ($\lambda_{qr}^{'e}$) component aligned with q coordinate is defined to zero. Then, the rotor flux λ_{r}^{e} is equal to λ_{dr}^{e}, the torque equation can be expressed as

$$(12) \qquad T_{em} = \frac{P}{2}\left(\lambda_{dr}^{'e} i_{qs}^{'e} \right)$$

where

$$(13) \qquad \lambda_{dr}^{'e} = \frac{L_m i_{ds}^{'e}}{1 + p\tau_r} \text{ or } \lambda_{dr}^{'e} = \frac{L_m i_{qs}^{e}}{\omega_{sl}\tau_r}$$
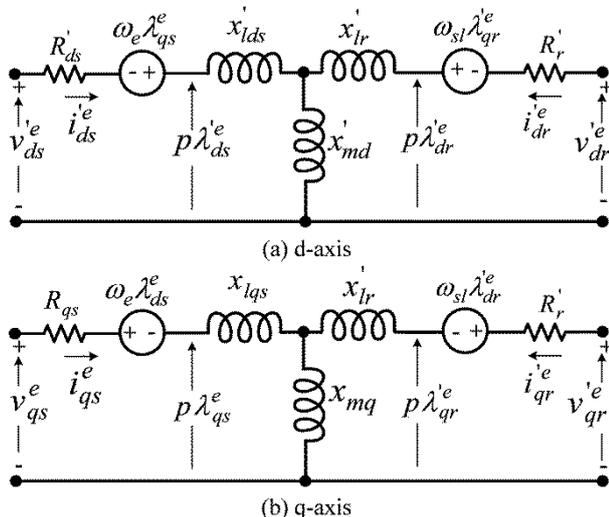

(a) d-axis

(b) q-axis

Fig. 7. Equivalent circuits of U-TPIM in a rotating reference frame: (a) Auxiliary winding variables referred to main winding in d-axis, (b) Main winding variables in q-axis.

For dynamic behavior, the torque production by the stator current i_{qs}^{e} is shown in Eq. (12). While, the stator current $i_{ds}^{'e}$ in Eq. (13) produces the rotor flux component. In addition, the slip speed can be calculated by Eq. (13). The over all of block diagram of indirect rotor flux oriented control for U-TPIM is presented in Fig. (8).
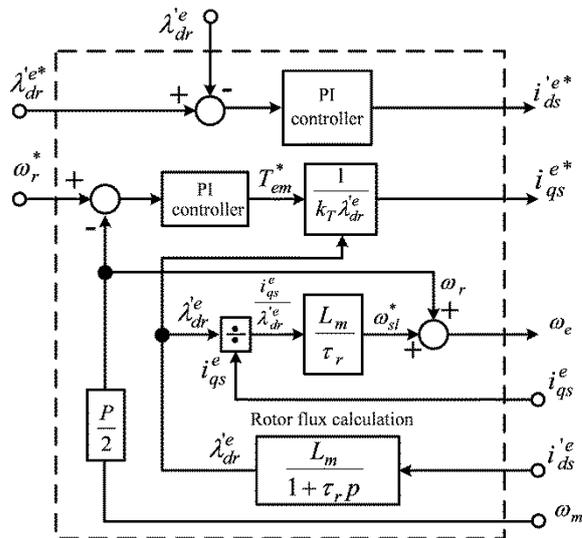

Fig. 8. Proposed block diagram of indirect rotor flux oriented control for U-TPIM.

To improve the performance of the current control by reducing the PI gains and the sensitive noise of a rotating reference frame transformation [17], [18] the feed-forward voltage components, $v_{ds\_comp}^{'e}$ and $v_{qs\_comp}^{e}$ need to be added into the output voltages of PI current controller as shown in Fig. (5). According to Fig. 7, the equivalent circuit of U-TPIM in a rotating reference frame, stator voltage equations in d-q axes are given as

$$(14) \qquad v_{ds}^{'e} = R_{ds}^{'} i_{ds}^{'e} + p\lambda_{ds}^{'e} - \omega_e \lambda_{qs}^{e}$$

$$(15) \qquad v_{qs}^{e} = R_{qs} i_{qs}^{e} + p\lambda_{qs}^{e} - \omega_e \lambda_{ds}^{'e}$$

Then, the feedforward voltage equations can be rearranged as

$$(16) \qquad v_{ds\_comp}^{'e} = -\omega_e \sigma_d L_s^{'} i_{qs}^{e} - R_r \frac{L_m}{L_r^2}\lambda_{dr}^{'e}$$

$$(17) \qquad v_{qs\_comp}^{e} = \omega_e \sigma_q L_s i_{ds}^{'e} + \omega_r \frac{L_m}{L_r}\lambda_{dr}^{'e}$$

Where, the leakage factors of d-q axes are

$$(18) \qquad \sigma_d = 1 - \frac{L_m^2}{L_r L_s^{'}} \text{ and } \sigma_q = 1 - \frac{L_m^2}{L_r L_s}$$

Proposed problems of unbalanced stator currents

Main and auxiliary windings are fed by an unbalanced voltage source. It is found that the magnitude of stator currents is unequal. As a result, the current transformation of stationary into rotating reference frame cannot be achieved because of occurring the double line frequency current. This is a major problem of the field oriented control of U-TPIM leading to the torque pulsation increasing. The problem of unbalanced stator current is explained as shown in Fig. 9. The current flowing through an auxiliary winding (i_{ds}^{s}) has a lower magnitude than the current flowing through a main winding (i_{qs}^{s}). For this reason, the current space vector trajectory i_s^s has a considerably elliptical part.

According to Fig. 9, for the unbalanced condition of the two stator currents, i_{ds}^{s} and i_{qs}^{s} are transformed into the rotating reference frame as

$$(19) \quad \begin{bmatrix} i_{ds}^e \\ i_{qs}^e \end{bmatrix} = \begin{bmatrix} \cos \omega t & \sin \omega t \\ -\sin \omega t & \cos \omega t \end{bmatrix} \begin{bmatrix} I_{ds} \cos(\omega t + \gamma) \\ I_{qs} \sin(\omega t + \gamma) \end{bmatrix}$$

Where, I_{ds}, I_{qs} are the magnitude of auxiliary and main winding currents, respectively. Form Eq. (19), stator current components in rotating reference frame can be expressed as

$$(20) \quad i_{ds}^e = \overbrace{\left(\frac{I_{ds} - I_{qs}}{2} \right) \cos(2\omega t + \gamma)}^{AC-Component} + \overbrace{\left(\frac{I_{ds} + I_{qs}}{2} \right) \cos \gamma}^{DC-Component}$$

$$(21) \quad i_{qs}^e = \overbrace{\left(\frac{I_{ds} - I_{qs}}{2} \right) \sin(2\omega t + \gamma)}^{AC-Component} + \overbrace{\left(\frac{I_{ds} + I_{qs}}{2} \right) \sin \gamma}^{DC-Component}$$
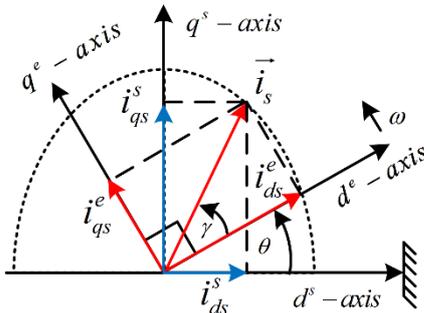

Fig. 9. Stator currents under unbalanced magnitude condition in stationary and rotating reference frame.

Unbalanced stator current waveforms in the stationary reference frame are shown in Fig. 10(a).
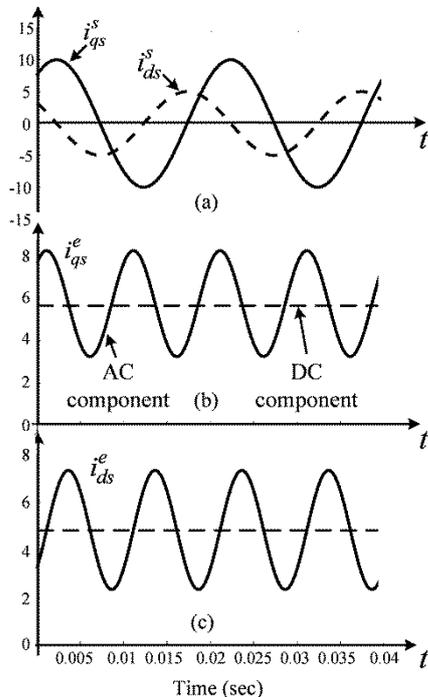

Fig. 10. Stator current in stationary into rotating reference frame transformation, (a) Unbalanced current flowing through the main and auxiliary winding (b) Oscillation current in d-axis (c) Oscillation current in q-axis.

Corresponding with stator current in Eq. (19), current transforming results in a rotating reference frame as shown in Eqs. (20) and (21) are plotted as Figs. 10 (b) and 10(c),

respectively. It can be seen that i_{ds}^e and i_{qs}^e consist of the AC and DC components implying that AC component superimposes on the DC current component. As mentioned in the previous section, i_{ds}^e and i_{qs}^e are flux and torque-producing currents. Consequently, the flux and torque pulsation will be greatly increased depending on the difference in both stator current magnitude. Note that the AC component is equal to zero if the magnitude of stator current is equal. In addition, unbalanced stator windings can also cause the increasing of backward torque and oscillation term of the electromagnetic torque. In order to solve these problems, the magnitude of stator currents need to be adjusted to equal before transformation into the rotating reference frame by suitable factor K_{eff} as shown in Fig. 5. As a result, double frequency and pulsating torque will be eliminated.

Rotor flux and electromagnetic torque estimation
As shown in Table 1. and Fig. 4, For the unsymmetrical U-TPIM parameters and its equivalent circuits in stationary reference frame, the stator voltage $v_{ds}^{'s}$ and v_{qs}^s are defined as $220 \angle 90^0$ V and $220 \angle 0^0$ V, respectively. The magnitude of stator currents in d-q-axes are calculated as 2.5 $\angle 32.57^0$ of $i_{ds}^{'s}$ and $2.62 \angle -59^0$ of i_{qs}^s, and the magnitude of rotor currents in d-q axes are calculated as -1.31 $\angle 86.94^0$ of $i_{dr}^{'s}$ and $-1.37 \angle -4.73^0$ of $i_{qr}^{'s}$, respectively. Then the instantaneous values by setting the $\omega_e t = 0$ of the stator and rotor current in d-q axes consisting of $i_{ds}^{'s}$, i_{qs}^s, $i_{dr}^{'s}$ and $i_{qr}^{'s}$ are equal to 2.11, 1.34, -0.07 and -1.36, respectively. Substituting the instantaneous current values of stator and rotor current into the electromagnetic torque in Eq. (6), then, the electromagnetic torque is equal to 2.22N.m. According to Fig. 4(b), when substituting the instantaneous current, magnetizing and leakage inductance into $\lambda_{dr}^{'s} = L_m i_{ds}^{'s} + \left(L_{lr}^{'} + L_m \right) i_{dr}^{'s}$, the instantaneous rotor flux vector calculation in d-axis is equal to 0.82Wb. In the same way in Fig. 4(a), the instantaneous rotor flux vector in q-axis is equal to -0.07Wb. The summation of the magnitude of rotor flux vector in d-q axes, $\lambda_r^{'s} = \sqrt{\left(\lambda_{dr}^{'s} \right)^2 + \left(\lambda_{qr}^{'s} \right)^2} = 0.82$, is set in rotor flux vector command for the proposed indirect rotor flux-oriented control.

TABLE 1. Parameters of proposed U-TPIM

Single phase motor 370W, 1375rpm, 4 Pole, 2.78A, C_B=8 μF C_A=12 μF , cos φ = 0.94, J = 0.011 kg.m², Turns ratio (K_{eff}) = 1.8		
Parameters	Stator winding in q-axis	Stator winding in d-axis
Voltage (rms)	220V	$220 \angle \pm 90^0$ V
Stator winding resistance	7.10 Ω	12.84 Ω
Stator leakage reactance	14.00 Ω	16.64 Ω
Rotor winding resistance	17.04 Ω	17.04 Ω
Rotor leakage reactance	14.00 Ω	14.00 Ω
Magnetizing reactance	126.40 Ω	126.40 Ω

Currents loop controller design
To calculate the gains of the proportional and the integral portions of PI controllers for the current control

loops, the frequency-response method is employed for calculating the current controllers for flux and torque production as shown in Fig. 11. Note that the feedforward voltage will not be significantly effect of the voltage response in d-q current loops, while it will be significantly effect for decreasing of the PI gain and sensitive noise voltage reduction [17]. For calculation, the feedforward voltage of proposed PI current loop controller will be neglected.
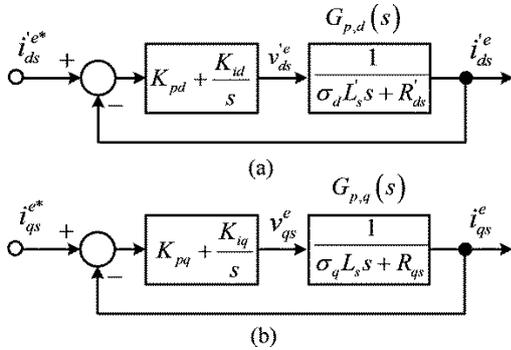

(a)

(b)

Fig. 11. Current-loop controller system (a) Current-loop for producing rotor flux in d-axis (b) Current-loop for producing torque in q-axis.

The frequency-response can be calculated by replacing "s" in the transfer function of plant by $j\omega_1$, where ω_1 is the crossover frequency. When the settling time and the phase margin are defined as 0.005 sec and 60 degrees, respectively. Then the crossover frequency for the stability control system can be obtained by [19]- [20].

(22) $\qquad \omega_1 = \dfrac{8}{t_s \tan\phi_M} = 923 \text{ rad/sec}$

Substitution the leakage factors σ_d, σ_q and other parameters are reported in Table 1 into plant equations as shown in Figs. 11 (a) and 11(b). For open loop transfer function of d-axis, the PI controller gain are calculated as $K_{pd} = 65$ and $K_{id} = 48,121$. Then, the current open-loop transfer function according with Fig. 11(a) can be written as

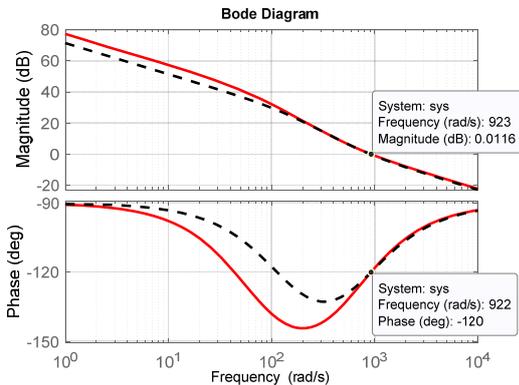(23) $\qquad G_d(s) = \dfrac{715(s + 740.32)}{s(s + 141.10)}$

Fig. 12. Bode diagram of d-q current control loops

Correspondingly, the PI gain of current control loop of q-axis are $K_{pq} = 84.34$ and $K_{iq} = 52,549.34$. According to Fig. 11(b), open loop transfer function can be given by

(24) $\qquad G_q(s) = \dfrac{767.50(s + 623.07)}{s(s + 64.54)}$

Bode diagrams of both open-loop transfer functions are shown in Fig. 12. Dash line and solid line are represented the current loop control in d and q axes, respectively.
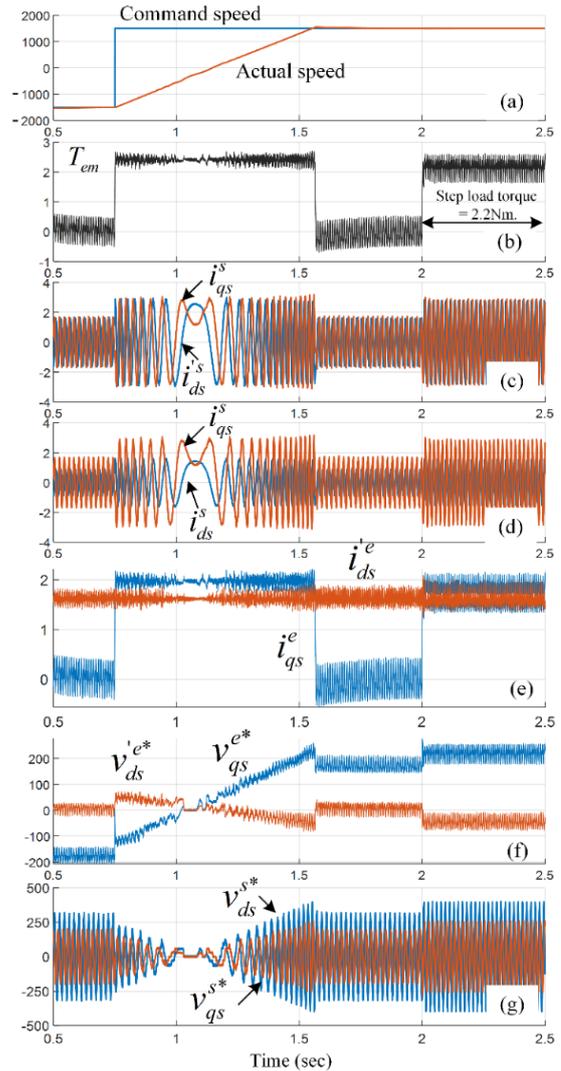

Fig. 13. Simulation results of indirect RFOC for U-TPIM at K_{eff} =1.8 (a) Command and actual speed at $\pm$ 1500rpm (b) Torque response while the reversed direction and step rated load torque 2.2 Nm. At 2 sec (c) Balanced stator currents before transformation to rotating reference frame (d) Main and auxiliary winding current waveform (e) Main and auxiliary winding current waveforms in rotating reference frame (f) Main and auxiliary winding voltage waveforms in rotating reference frame (g) Fundamental voltage across main and auxiliary windings.
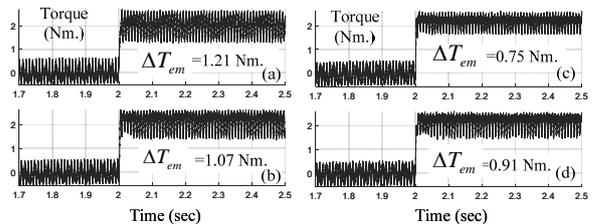

Fig. 14. Torque transient responses and torque ripples at step rated load torque = 2.2Nm. (a) K_{eff} =1.6 (b) K_{eff} =1.7 (c) proposed K_{eff} =1.8 (d) K_{eff} =1.9.

From Fig. 13(c), the stator current in terms of a stationary reference frame transformed into the rotating

reference frame is shown in Fig. 13(e). Fig 13(f) illustrates d-q voltage command waveforms in terms of rotating reference frame tramsformation. Results from Fig 13(f), d-q stator voltages in rotating reference are transformed into the stationary reference frame. Afterward, v_{ds}^{s*} is only multiplied by factor K_{eff} as shown in Fig. 13(g). According to all these results, they confirm that the proposed method can be implemented correctly. Especially, the correct proportion of factor K_{eff} leads to a reduction in torque ripple in accordance with simulation results in Fig. 14. For the torque ripple simulation results at step load torque between the time of 2-2.5sec, it can be seen that the torque ripple reduction of factor K_{eff} =1.8 is lowest in accordance with the test result calculation. For other factors, K_{eff} give poor performance.

From Fig. 13(c), the stator current in terms of a stationary reference frame transformed into the rotating reference frame is shown in Fig. 13(e). Fig 13(f) illustrates d-q voltage command waveforms in terms of rotating reference frame tramsformation. Results from Fig 13(f), d-q stator voltages in rotating reference are transformed into the stationary reference frame. Afterward, v_{ds}^{s*} is only multiplied by factor K_{eff} as shown in Fig. 13(g). According to all these results, they confirm that the proposed method can be implemented correctly. Especially, the correct proportion of factor K_{eff} leads to a reduction in torque ripple in accordance with simulation results in Fig. 14. For the torque ripple simulation results at step load torque between the time of 2-2.5sec, it can be seen that the torque ripple reduction of factor K_{eff} =1.8 is lowest in accordance with the test result calculation. For other factors, K_{eff} give poor performance.

Experimental results

The hardware prototype and schematic diagram of the proposed indirect RFOC for U-TPIM drive are illustrated in Fig. 15 and Fig. 16, respectively.
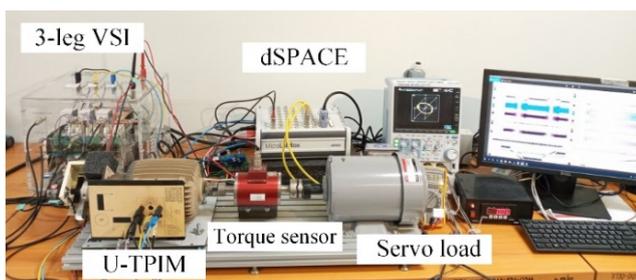

Fig. 15. Photograph of the experimental setup for the proposed U-TPIM drive.

The rig consists of an unbalanced two-phase induction motor and power voltage source inverter modulated by unbalanced SVPWM technique using dSPACE MircoLab Box together with Matlab/Simulink. The result waveforms are recorded by the dSPACE control-desk software. The voltage source inverter employs IGBTs as switching devices. The carrier switching frequency is 10kHz, and the sampling time is equal to 100 μs. To verify the correct proposed method, the test conditions are divided into two parts for instance the dynamic performance of indirect rotor

field-oriented control at properly factor K_{eff} =1.8 and to adjust the factor K_{eff} between 1.6-1.8 in order to compare the torque ripple reduction by the same PI current controller parameter gains in each condition. According to Eq. (10) the DC bus voltage with regard to voltage across main and auxiliary winding, DC bus voltages at factor K_{eff} =1.6, 1.7 and 1.8 are calculated as 587V, 613V and 640V, respectively.
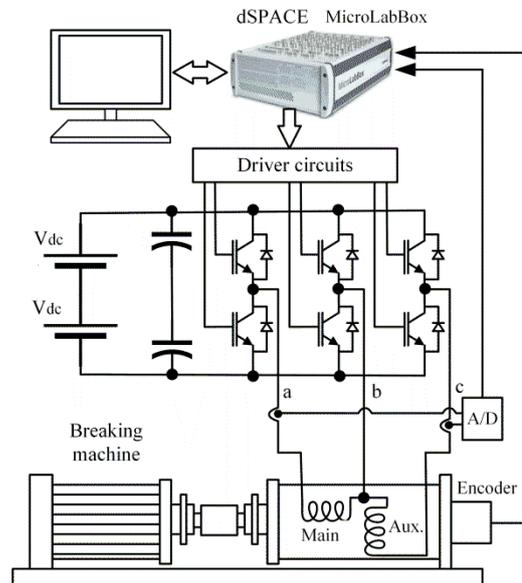

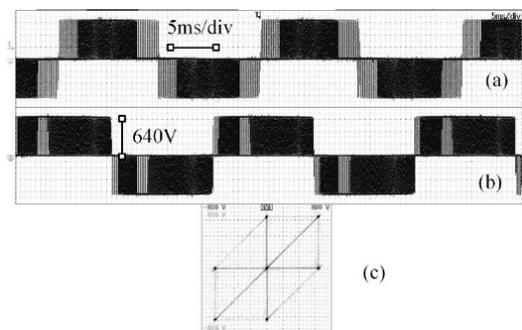Fig. 16. Schematic diagram of the proposed U-TPIM drive.

Fig. 17. Experimental PWM output voltage waveforms at K_{eff} = 1.8; (a) Main winding voltage (b) Auxiliary winding voltage (c) Location of active space vectors in d-q plane.
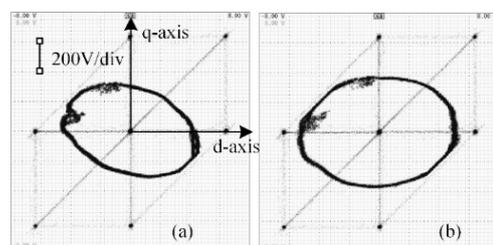

Fig. 18. Voltage vector trajectory for the unbalanced applied voltage at K_{eff} = 1.8; (a) No load torque (b) Under load torque=2Nm.
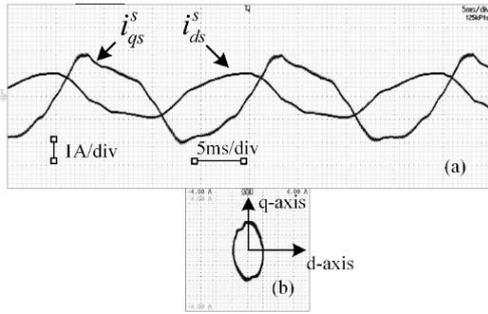
Fig. 19. Measured stator currents at no-load torque condition (a) Main and auxiliary winding current (b) Ellipse trajectory of current vector at K_{eff} = 1.8.
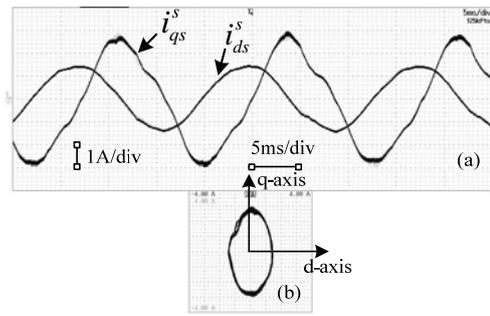

Fig. 20. Measured stator currents under load torque = 2Nm. (a) Main and auxiliary winding currents (b) Ellipse trajectory of current vector at K_{eff} = 1.8.
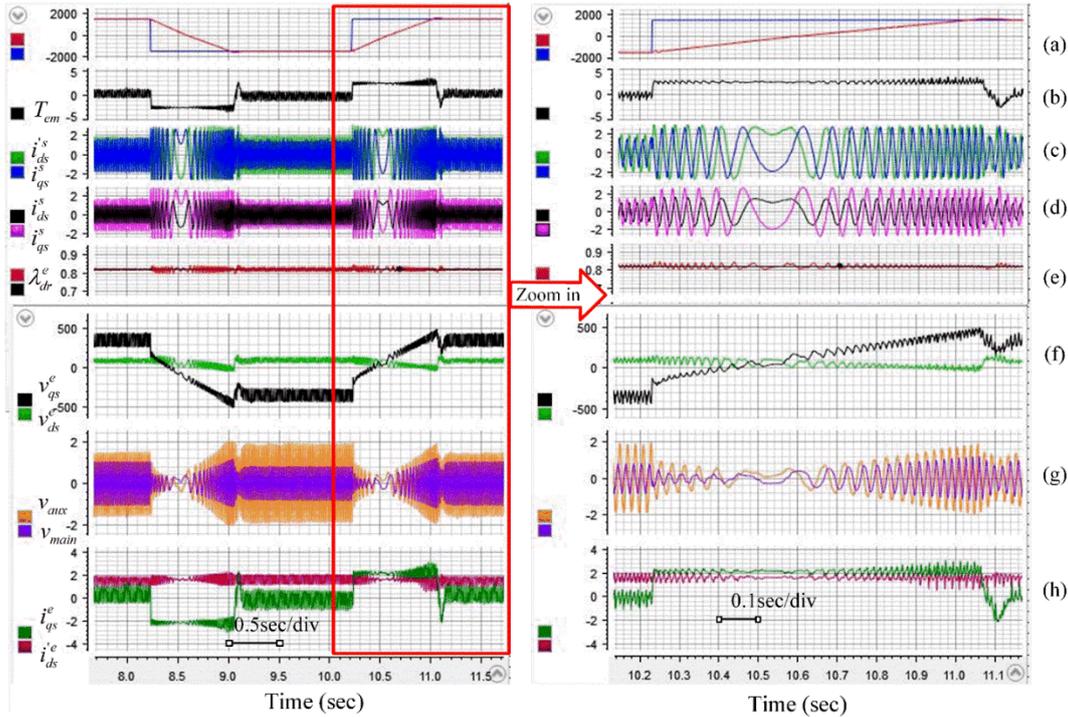

Fig. 21. Experimental results by dSPACE Control Desk of indirect RFOC for the U-TPIM implementation at K_{eff} =1.8 with zoom in details

(a) Command and actual speeds at $\pm$ 1500rpm (b) Electromagnetic torque response (c) Balanced stator currents before transformation to rotating reference frame (d) Main and auxiliary winding current waveform (e) Rotor flux (f) Main and auxiliary winding voltage waveforms in rotating reference frame (g) Fundamental voltage across main and auxiliary windings (h) Main and auxiliary winding current waveforms in a rotating reference frame.
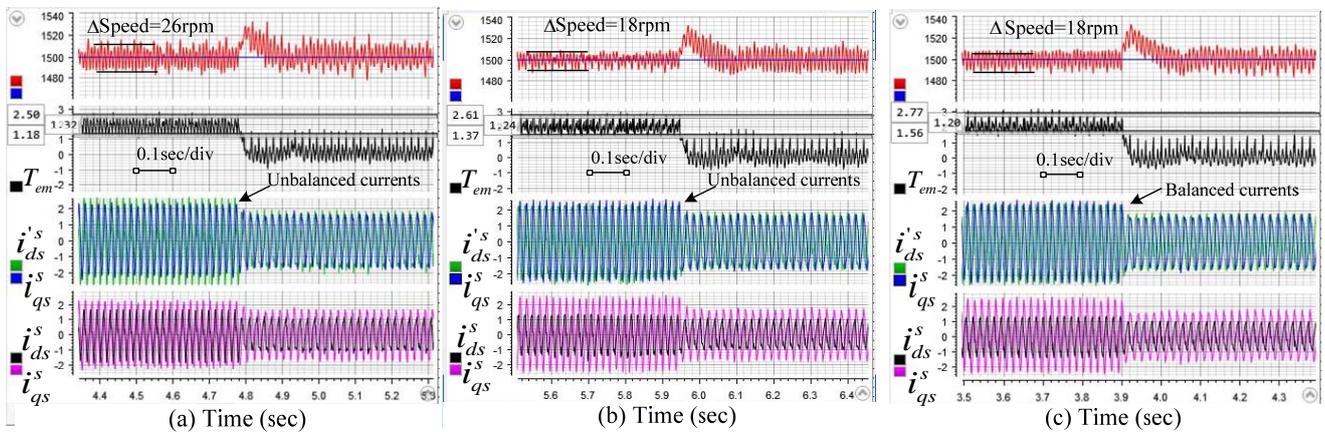

Fig. 22. (a) Measured rotor speed, electromagnetic torque (ΔT_{em} =1.32Nm.), d-q axis currents at K_{eff} = 1.6 and DC bus voltage = 587V.

(b) Measured rotor speed, electromagnetic torque (ΔT_{em} =1.24Nm.), d-q axis currents at K_{eff} = 1.7 and DC bus voltage = 613V.

(c) Measured rotor speed, electromagnetic torque (ΔT_{em} =1.20Nm.), d-q axis currents at K_{eff} = 1.8 and DC bus voltage = 640V.

Closed-loop control corresponding with indirect rotor field oriented control system in Fig. 5 at no-load, 1500rpm and K_{eff} =1.8, Figs. 17(a) and 17(b) illustrate PWM voltage waveforms of the main and auxiliary winding voltages, and Fig. 17(c) shows the location of the active space vector in d-q plane. Both fundamental voltages are plotted in x-y graph by superimposed on the space vector in the d-q plane as shown in Fig 18(a). This confirms in the results that the voltage vector trajectory is an ellipse locus. It implies that the auxiliary winding voltage has more magnitude than the main winding voltage. When considering the voltage vector trajectory under load torque at 2Nm. as shown in Fig. 18(b), the voltage vector trajectory has remained in the ellipse locus. It can be seen that a voltage vector trajectory under load torque is bigger than no-load torque condition, and phase shift angle between both fundamental voltages are kept constant at 90 degrees. Figs. 19 and 20 illustrate experimental stator currents at no-load and under load torque conditions, respectively. Both of the current vectors yield an ellipse trajectory. It can be seen that the magnitude currents of no-load and under load torque are different about 1.8 times in the same manner as the difference of magnitude voltages of auxiliary and main windings, because the factor K_{eff} is adjusted at 1.8. Fig. 21 shows the performance evaluation of indirect RFOC according to the block diagram shown in Figs. 5 and 8. To successfully carry out the optimal rotor field oriented control of the U-TPIM, for the hardware implementation, all of available parameters of experimental results are calculated the same method as the simulation parameters so as to verify correctness of proposed method. Fig. 21 compares the performance of speed, torque capability, stator current waveforms in the d-q axes and zoom into its waveforms. It is noted that balanced and unbalanced zones can be completely separated by factor K_{eff} =1.8. In addition, the experimental results show that rotor flux oriented system can be performed in four quadrants operation like a symmetrical two-phase motor drive. If factor K_{eff} is less or greater than 1.8, the magnitude currents in balanced zone will be changed as in the unbalanced magnitude currents. For this reason, the AC double line frequency terms will be generated in rotating reference frame transformations leading to an increase in torque pulsation. Fig. 22 compare the torque ripple and stator current in each factor K_{eff} variation against the load torque at 2Nm and +1500rpm. It is found that the lowest speed and torque ripple occur at K_{eff} =1.8. Because magnitude of d-axis and q-axis currents in stationary reference is almost symmetry.

Conclusion

This paper aims to control the indirect rotor field-oriented of unsymmetrical two-phase induction motor supplied with unbalanced two-phase output by a three-leg voltage source inverter. This proposed method and experimental results show that U-TPIM can be controlled as the variable speed drive as same as the three-phase induction motor. Since impedance parameters of unsymmetrical two-phase induction motor are unequal, main and auxiliary winding voltages need to be applied the unbalanced voltage source in order to change the unbalanced equivalent circuits of the U-TPIM to symmetrical equivalent circuits by defining the suitable factor K_{eff}. Moreover, the factor K_{eff} is the most important factor not only change to an almost symmetrical parameter component of equivalent circuits in the d-q axes of U-TPIM but also to reduce AC double line frequency component owing to balanced stator currents in rotating reference

frame transformation. If the factor K_{eff} is not suitable in more or less than the determined value, then the torque and speed ripple will be increased. Apparently, all of simulation and experimental results verify the correctness and improvement of the U-TPIM drive performance.

Authors: Mr.Piya Sirikan. E-mail: sirikanp@gmail.com; Assoc.Prof.Dr.Chakrapong Charumit, E-mail: c.charumit@gmail.com, Department of Electrical Engineering, Pathumwan Institute of Technology, 833 Rama1 Wangmai District, Bangkok, Thailand.

REFERENCES

[1] Holmes D.G., Kotsopoulos A., Variable speed control of single and two phase induction motors using a three phase voltage source inverter, *Conference Record of the 1993 IEEE Industry Applications Conference Twenty-Eighth IAS Annual Meeting*, Toronto, ON, Canada, (1993), 613–620

[2] Gangadhar P.N., Banchhor D.K., Dhabale A., Torque ripple reduction in unsymmetrical two phase induction motor, *2018 IEEE International Conference on Power Electronics, Drives and Energy Systems (PEDES)*, Chennai, India, (2018), 1-6

[3] Charumit C., Kinnares V., Realization of a carrier-based unbalanced output space vector PWM strategy using analogue and digital techniques for three-leg voltage source inverter fed two-phase induction motors, *IEEJ Trans. Industry Applications*, 129(2009), No. 6, 636–648

[4] Kumsuwan Y., Premrudeepreechacharn S., Kinnares V., A Carrier-Based Unbalanced PWM Method for Four-Leg Voltage Source Inverter Fed Unsymmetrical Two-Phase Induction Motor, *IEEE Trans. Industrial Electronics*, 60(2013), No. 5, 2031–2041

[5] Piyarat W., Hothongkham P., Charumit C., Kinnares V., Simple speed control of an asymmetrical type two-phase induction motor drive, *International Conference on Electrical Engineering/ Electronics, Computer, Telecommunications and Information Technology*, Chiang Mai, Thailand, (2010), 274-278

[6] Abdel-Rahim N.M., Shaltout A.A., Slip-frequency control of single-phase induction motor operated as two-phase motor, *30th Annual Conference of IEEE Industrial Electronics Society*, 2(2004), 1417–1422

[7] Abdel-Rahim N.M.B., Shaltout A., An Unsymmetrical two-phase induction motor drive with slip-frequency control, *IEEE Trans. on Energy Conversion*, 24(2009), No. 3, 608–616

[8] Charumit C., Kinnares V., Discontinuous SVPWM techniques of three-leg VSI-fed balanced two-phase loads for reduced switching losses and current ripple, *IEEE Trans. Power Electronics*, 30(2015), No. 4, 2191–2204

[9] Correa M.B.R., Jacobina C.B., da Silva E.R.C., Lima A.M.N., Vector control strategies for single-phase induction motor drive systems, *IEEE Trans. on Industrial Electronics*, 51(2004), No. 5, 1073–1080

[10] Vaez-Zadeh S., Reicy Harooni Sh., Decoupling vector control of single-phase induction motor Drives, *2005 IEEE 36th Power Electronics Specialists Conference*, Dresden, Germany, (2005), 733–738

[11] Nied A., de Oliveira J., de Sá F.L., de F. Campos R., de C. Stival L.H.R., Single-phase induction motor indirect field oriented control under nominal load, *International Conference on Power Electronics and Drive Systems (PEDS)*, Taipei, Taiwan, (2009), 789–793

[12] Jang D.H., Problems Incurred in a Vector-controlled single-phase induction motor, and a proposal for a vector-controlled two-phase induction motor as a Replacement, *IEEE Trans. on Power Electronics*, 28(2013), No. 1, 526-536

[13] Matsch L.W., Morgan J.D., Electromagnetic and electromecha-nical machines, *John Wiley & Sons*, 3rd ed., (1988), 289-303

[14] Krause P.C., Wasynczuk O., Sudhoff S.D., Analysis of electric machinery and drive systems, *Wiley-IEEE Press*, 2nd ed., (2002), 361-393

[15] Ong C.M., Dynamic simulation of electric machinery using matlab/simulink, *Prentice Hall PTR*, (1998), 214-221

[16] Trzynadlowski A.M., The field orientation principle in control of induction motors, *Kluwer academic publishers*, (1994), 97-108

[17] Kim S.H., Electric motor control DC, AC and BLDC motors, *Elsevier Science*, (2017), 256-263

[18] Feraga C.E., Bouldjedri A., Indirect rotor field oriented control strategy for single phase induction motor drives, *Przegląd Elektrotechniczny*, 88(2012), nr. 12, 222–225

[19] Phillips C.L., Harbor R.D., Feedback control system, 4th ed., *Prentice Hall*, (2000)

[20] Sirikan P., Charumit C., Implementation of indirect rotor field oriented control for three-phase induction motor drive based on TMS320F28335 DSP, *Przegląd Elektrotechniczny*, 96(2020), nr. 9, 153–158